Nonlinear dynamic perspectives on dynamic force microscopy

S. I. Lee [a], S. W. Howell [b], A. Raman [a,*], R. Reifenberger [b]

[a] *School of Mechanical Engineering, Purdue University, West Lafayette, IN 47907, U. S. A.*

[b] *Department of Physics, Purdue University, West Lafayette, IN 47907, U. S. A.*

Abstract

Dynamic force microscopy (DFM) utilizes the dynamic response of a resonating probe tip as it approaches and retracts from a sample to measure the topography and material properties of a nanostructure. We present recent results based on nonlinear dynamical systems theory, computational continuation techniques and detailed experiments that yield new perspectives and insights into DFM.

A dynamic model including van der Waals and Derjaguin-Müller-Toporov contact forces demonstrates that periodic solutions can be represented as a catastrophe surface with respect to the approach distance and excitation frequency. Turning points on the surface lead to hysteretic amplitude jumps as the tip nears/retracts from the sample. New light is cast upon sudden global changes that occur in the interaction potential at certain gap widths that cause the tip to "stick" to, or tap irregularly the sample. Experiments are performed using a tapping mode tip on a graphite sample to verify the predictions.

Key words: Dynamic force microscopy; Tapping mode; Nonlinear dynamics; Bifurcation
PACS: 68.35.Ja, 05.45.-a, 68.37.Ps

1 Introduction

The study of the variation of interaction force with separation between an atomic force microscope tip and sample is of fundamental importance in nanoscience. Traditionally this is performed in the static mode where the

* Corresponding author
Email address: raman@ecn.purdue.edu (A. Raman).

deflection of the cantilever is monitored as it approaches and retracts from the sample. Dynamic force microscopy (DFM) uses a resonating tip to approach and retract from the sample. The measurement of the amplitude and phase of the resonating tip during approach and retraction has been used to measure viscoelastic losses in the sample [1], material properties of samples in liquids [2], and in air [3]. Because the tapping mode phase response is sensitive to sample elasticity, it can be used to image multi-component specimens with negligible difference in topography but substantial difference in elasticity. Developing a fundamental understanding of DFM response also aids the optimization of tapping mode phase imaging for multi-component samples [4] and soft biomolecules [5].

The underlying dynamics of the resonating microcantilever during approach and retraction is highly nonlinear and has been investigated by a number of authors [4,6–9]. The main conclusions of these previous works can be summarized as (i) sharp jumps can occur at certain separations in the vibration amplitude and phase response as the resonating tip approaches the sample, (ii) these jumps can occur during retraction at different separations leading to reproducible hysteresis, (iii) the occurrence of these jumps is excitation frequency dependent, that is, for some frequency no jumps may occur while for frequencies just above and below resonance hysteresis occurs but at different tip sample separations, (iv) it has been demonstrated that the presence of jumps indicates a switching between two different co-existing periodic solutions, one operating in the attractive interaction force regime and another in the repulsive force regime, and (v) the magnitude of the jumps in the phase response (which are a measure of the phase imaging contrast) during approach and retraction are dependent on the cantilever stiffness, adhesion and sample elasticity.

The above literature, however, does not describe the behavior of DFM at very small separations when the tip can stick to the sample or vibrate irregularly. Moreover the previous studies do not include all time dependent terms that are inherent in the dither excited microcantilever and also are based on numerical simulations which cannot detect unstable solutions. The first contribution of the present work is to address these outstanding issues rigorously, using models that include all time dependent terms and modern continuation tools to track stable and unstable periodic motions. Another group of papers addresses the the nonlinear response of the tapping mode AFM microcantilever with *fixed approach distance* but with varying frequencies [10–13]. To date, however, a clear connection has not been established between the nonlinear response observed during the fixed approach distance, varying frequency scenario and the nonlinear response for fixed frequency, varying approach distance (DFM) scenario. In this regard, the second contribution of this paper is to explain this connection using the concept of bifurcation sets. Finally, we perform experiments using a Si tip and HOPG sample to demonstrate a close agreement

between theoretical predictions and experimental response.

2 Modeling and equilibrium solutions

2.1 Tip-sample interactions and equation of motion

To analyze the tip-sample interaction in DFM, van der Waals and Derjaguin-Mueller-Toporov (DMT) contact [14] forces (F_{vdW}, F_{DMT}) between a sphere (tip apex) and a flat surface (sample) are assumed. We use van der Waals forces when tip is separated from the sample (Figure 1(a)).

$$F_{vdW}(z) = -\frac{AR}{6\,z^2}, \quad (\text{for } z > a_0) \tag{1}$$

where A is the Hamaker constant, R is tip radius, and z is the instantaneous tip-sample gap. When the tip contacts the sample (Figure 1(b)), according to the DMT contact model

$$F_{DMT}(z) = -\frac{AR}{6\,a_0^2} + \frac{4}{3}E^*\sqrt{R}\,(a_0 - z)^{3/2}, \ (\text{for } z \le a_0) \tag{2}$$

where E^* is the effective elastic modulus which is determined by

$$\frac{1}{E^*} = \frac{1-\nu_{tip}^2}{E_{tip}} + \frac{1-\nu_{sample}^2}{E_{sample}},$$

where E_{tip}, ν_{tip}, and E_{sample}, ν_{sample} are respectively the Young's modulus and Poisson's ratio of tip and sample. a_0 is the intermolecular distance [12] at which contact is initiated. The interaction force as a function of approach distance is plotted in Figure 2 using Equations (1) and (2) for specific sample-tip properties listed in Table 1. The attractive (negative) interaction is primarily due to the van der Waals forces while the repulsive interactions arise from the DMT contact forces.

2.2 Nonlinear static equilibrium

First the static cantilever deflection without dynamic excitation is computed by solving for the equilibrium gap between tip and sample (η^* in Figure 5(a)) in the presence of the nonlinear interaction forces. Let Z be the approach distance (see Figure 5). The equilibrium gap can be calculated as a function

of approach distance Z through balance of the cantilever restoring force and the tip-surface interaction forces.

$$k(Z - \eta^*) = F_i(\eta^*), \tag{3}$$

where k is the bending stiffness coefficient of the microcantilever, and F_i is the total tip-sample interaction forces combined by F_{vdW} and F_{DMT}. Solving the equation (3) for different Z yields the equilibrium gap between the tip and sample η^*, as a function of Z. The Liapunov stability of an equilibrium is computed easily using the Lagrange-Dirichlét theorem [1].

Figure 3 shows the equilibrium solutions for the tip deflection and their stability. For the nonlinear equilibrium solutions, we use the values listed in Table 1. As is well known the tip snaps into contact on approach and snaps off on retraction. This divides problem into two regimes: *monostable* far from sample and *bistable* close to sample where two stable and one unstable equilibria coexist.

The dynamics of the microcantilever in *monostable* and *bistable* region are significantly different with distinct nonlinear behaviors and unique instability mechanisms. This will be demonstrated in the following sections in detail using a single mode discretization of the microcantilever-sample system. However to illustrate the point at this stage, the total potential energy wells of the discretized model are plotted in Figure 4 for $Z = 5$ nm and 30 nm corresponding respectively to *bistable* and *monostable* region. The total potential energy is an asymmetric two-well potential in *bistable* region (Figure 4(a)), while it is a single well potential in *monostable* region (Figure 4(b)). In both cases the tip-sample contact leads to non-smoothness of the potential well. The equilibrium closer to the sample corresponds to a state where the tip is effectively stuck to the sample. Note also that the forced vibration responses of the tip in these two potential wells are expected to be very different.

2.3 Dynamic equation

The dynamic equation of motion of tip deflection $u(t)$ about its equilibrium subject to base harmonic motion $Y \sin \Omega t$ from the dither piezo can be derived through a single mode discretization of the continuous cantilever model. Writing the equations of motion of the vibrating microcantilever in a *non-inertial reference frame* attached to the base of the microcantilever leads to

[1] The stability can be determined by examining the sign of the second derivative of the total potential energy (sum of the cantilever elastic energy and the interaction potential) evaluated at that equilibrium.

the following representation of the vibrations about the equilibrium

$$\begin{aligned}&\rho_c A_c \ddot{u}(x,t) + E_c I_c (u''''(x,t) + w^{*''''}(x)) \\ &\quad = F_i(Z - w(L,t))\delta(x-L) + \rho_c A_c \Omega^2 Y \sin\Omega t.\end{aligned} \tag{4}$$

The equation (4) is highly nonlinear, and non-autonomous and its discretization may be achieved suitably through a projection of the dynamics onto the linear modes of the system. However, the linear modes and frequencies of the microcantilever about its static equilibrium are different from those of a microcantilever located far from the sample surface [15]. Using the Galerkin method [16], the vibration modes and frequencies of the microcantilever with the spring-coupled end [17] about the chosen nonlinear equilibrium (a specific position on the stable equilibrium solution in Figure 3) are computed.

Consider now the situation when the excitation frequency Ω in equation (4) is close to the lowest natural frequency ω_1 of the microcantilever about its elastostatic equilibrium. Under near-resonant forcing, only one mode of the microcantilever is assumed to participate in the response

$$u(x,t) = \Phi_1(x) q_1(t), \tag{5}$$

where $\Phi_1(x)$ is the first eigenfunction of the cantilever about the chosen equilibrium and $q_1(t)$ is the time dependent generalized coordinate. Substitution of equation (5) into equation (4), and on taking inner products of the resulting equations with $\Phi_1(x)$ yields the the dimensionless ordinary differential equation of motion of the tip

$$\frac{\mathrm{d}^2\bar{\eta}}{\mathrm{d}\tau^2} + D(\bar{z})\frac{\mathrm{d}\bar{\eta}}{\mathrm{d}\tau} + \bar{\eta} = -C_1 + \bar{F}_i(\bar{z}) + B\bar{\Omega}^2\bar{y}\sin\bar{\Omega}\tau, \tag{6}$$

where

$$\bar{\eta} = \frac{u(L,\tau)}{\eta^*}, \quad \bar{y} = \frac{Y}{\eta^*}, \quad \bar{\Omega} = \frac{\Omega}{\omega_1}, \quad \tau = \omega_1 t, \quad B = \frac{\Phi_1(L)\int_0^L \Phi_1 \mathrm{d}x}{\int_0^L \Phi_1^2 \mathrm{d}x},$$

$$D(\bar{z}) = \begin{cases} D_1, & (\text{for } \bar{z} > \bar{a}_0) \\ D_2, & (\text{for } \bar{z} \le \bar{a}_0) \end{cases}$$

$$\bar{F}_i(\bar{z}) = \begin{cases} C_1/\bar{z}^2, & (\text{for } \bar{z} > \bar{a}_0) \\ C_1/\bar{a}_0^2 + C_2\left(\bar{a}_0 - \bar{z}\right)^{3/2}, & (\text{for } \bar{z} \le \bar{a}_0) \end{cases}$$

$$D_1 = \frac{1}{Q}, \quad C_1 = -\frac{AR\ \Phi_1^2(L)}{6\,(\eta^*)^3\,{\omega_1}^2\rho_c A_c \int_0^L \Phi_1^2 \mathrm{d}x}, \quad C_2 = \frac{4E^*\sqrt{R\eta^*}\ \Phi_1^2(L)}{3{\omega_1}^2\rho_c A_c \int_0^L \Phi_1^2 \mathrm{d}x},$$

$$\bar{z} = 1 - \bar{\eta}(\tau) - \bar{y}\sin\bar{\Omega}\tau, \quad \text{and} \quad \bar{a}_0 = \frac{a_0}{\eta^*}.$$

Note that equations (4) and (6) are written in a non-inertial frame attached to the moving base, and the instantaneous gap $\bar{z}$ clearly depends on base motion $\bar{y}\sin\bar{\Omega}\tau$. Therefore the base excitation appears as an external forcing term as well as in time dependent terms in the interaction forces F_i. These additional terms have mostly been ignored in the literature [10–13,18–21]. Finally note that the modal damping $D(\bar{z})$ has been included in the discretized model. The modal damping is piecewise constant and models the different dissipation mechanisms acting on the microcantilever while it is in or out of contact with the sample. While the damping due to surrounding air has been modelled traditionally as a linear viscous term, the dissipation mechanisms during contact are far more complicated [22,23] and involve the consideration of liquid bridges and phonon scattering. In order to retain the simplicity of the discretized model while retaining to an extent the difference between dissipation mechanisms in air and during contact, we introduce a two step modal damping. D_1 is the modal damping coefficient in air and can be calculated from the Q factor of linear vibration far from the sample, while D_2 is the resultant modal damping during the duration of tip contact with the sample.

2.4 Tip-sample properties

All the key system parameters needed for the static equilibria as well as for the nonlinear dynamics computations are listed in Table 1. Some of system parameters listed in Table 1 are obtained from the linear vibration experiments performed far from the sample, while other properties are taken from the literature. Resonance frequency f_1 and Q factor are obtained from the experimental frequency response of the microcantilever without sample. The tip radius R, cantilever stiffness k, and cantilever geometric dimensions (length, width, and thickness) are taken from the manufacturer's catalog (http://www.olympus.co.jp) of the microcantilever (OMCL-AC240TS) used in the experiment. Cantilever material density ρ_c, Young's modulus E_c and effective elastic modulus E^* are based on typical values for silicon and graphite using Poisson's ratio of 0.3 [24]. The Hamaker constant A between Si and HOPG is derived from the values of silicon-air and graphite-air Hamaker constants which are found in the literature [25]. Further, the intermolecular distance a_0 is fitted from the static force-approach distance curve. The modal damping is implemented using the piecewise constant model described earlier. Accordingly $D_1 = 0.015$ (from the Q factor in linear vibration response far

from the surface) and $D_2 = 4.0$ during contact (this value is used in order to fit the frequency extent of the saturated amplitude region in one set of experiments). It may be emphasized here that none of the chosen parameter values used for the computation except a_0 and D_2 are fitted to match the nonlinear experimental data.

For the system under consideration, we use the values listed in Table 1. Use of these parameter values yields the nondimensionalized, discretized model (Equation (6)) of the single mode response about the chosen equilibrium with specific coefficients: (i) $D_1 = 0.015$, $D_2 = 4.0$, $C_1 = 3.15037 \times 10^{-6}$, $C_2 = 3.31287 \times 10^2$, $B = 1.71955$, and $\bar{y} = 0.0145$ in *monostable* region (at $Z = 60$ nm); and (ii) $D_1 = 0.015$, $D_2 = 4.0$, $C_1 = 5.5134 \times 10^{-3}$, $C_2 = 95.515$, $B = 1.71983$, and $\bar{y} = 0.175$ in *bistable* region (at $Z = 5$ nm).

3 Experimental and computational techniques

3.1 Experimental techniques

To demonstrate the effects of nonlinearities on the DFM response, a commercially available air-AFM produced by NanoTec^{TM}was chosen to perform these experiments. An Olympus^{TM}diving-board silicon cantilever(resonance frequency 52.4 kHz, Q $\approx$ 66.7) was employed. The experimental setup is displayed in Figure 6. In order to perform experiments on the nonlinear response of the cantilever, it is necessary to have control of the approach distance as the frequency of excitation is systematically varied. The amplitude and phase of the cantilever response must be rapidly measured as a function of the excitation frequency. In general, this is difficult to achieve in commercial scanning probe systems and requires the use of a flexible software system. In our case, we used the WSxM software available from NanoTec^{TM}.

The standard AFM control system is used to bring the tip to a distance $\sim$200 nm above the sample while operating the AFM in non-contact mode. After the initial coarse approach, the frequency response of the cantilever is measured systematically as a function of decreasing approach distance. This is accomplished by rerouting the control of the Z segment of the AFM's piezotube to a digital-to-analog converter (DAC) onboard the lock-in amplifier. The DAC provides the voltage required to control the Z expansion of the piezotube. The expansion of the piezotube as well as the driving frequency of the cantilever are controlled by the lock-in *via* a general-purpose interface bus (GPIB) controller. The GPIB software controls the voltage step applied to the high voltage power supply of the piezotube, the frequency used to drive the cantilever, and the measurement of the cantilever oscillation.

Two types of experiments were performed. In the first for each tip-sample approach distance, the excitation frequency (Ω) is increased from a starting frequency to a final frequency ($\Omega_i \rightarrow \Omega_f$) across microcantilever's linear resonance frequency (ω_1). Then the frequency is decreased across resonance from Ω_f to Ω_i. For each frequency increment (Δf), the amplitude and phase of the cantilever oscillation referenced to the excitation frequency are measured by the lock-in amplifier. Following this approach, the tip-sample approach distance is reduced in increments until the cantilever oscillation displays non-linear resonance behavior, indicating that the tip is tapping the sample. By plotting the amplitude and phase response of the cantilever as a function of Z, it is possible to map out the entire non-linear response of the cantilever.

In the second type of experiment, the amplitude of the cantilever oscillation at a fixed frequency of excitation Ω was measured as a function of tip-sample approach distance Z. For this experiment the flexible NanoTec$^{\mathrm{TM}}$control system (now controlling the Z-piezotube) was used to simultaneously measure the static deflection of the cantilever and the cantilever oscillation amplitude (*via* the lock-in amplifier) as the cantilever tip was brought into contact with the sample surface. This procedure generated both the force vs. Z and amplitude vs. Z curves. These measurements were made for a number of different oscillation frequencies between $\omega_1 \pm 2$ kHz.

3.2 Computational techniques

AUTO 97, a publicly available continuation and bifurcation program for differential equations is used to continue periodic orbits of the equation (6). AUTO 97 uses sophisticated pseudo-arc length continuation and accurate Floquet multiplier calculations to follow both stable and unstable periodic solutions. Bifurcations of periodic orbits including period doubling and periodic folds (global saddle-node bifurcations) can be detected and continued conveniently in AUTO 97. The response often contains higher harmonics and the phase of the response with respect to the excitation is then computed using the first harmonic of the response. To avoid the mathematical complications in the computation of Floquet multipliers due to non-smooth interaction forces at $z = a_0$, we use a smooth, cubic interpolation in a thin "boundary" layer about $z = a_0$.

The periodic orbits of equation (6) for the fixed approach distance, varying frequency case are computed using the excitation frequency as a primary continuation parameter in AUTO. However, it is practically impossible to obtain the DFM responses for the fixed frequency, varying approach distance case in AUTO using the approach distance Z as a primary continuation parameter. This is because the equilibrium gap η^* and the natural frequencies and mode

shapes of the microcantilever need to be computed separately for each Z. To address this problem, we compute for each Z separately, the the response for the fixed approach distance, varying frequency case as described earlier. Finally, these responses for different Z can be assembled together to compute the nonlinear behavior in DFM.

4 Nonlinear response and bifurcation sets

4.1 Response in monostable region

First let us consider the experimental and computed response in the *monostable* region. The peak-to-peak amplitude and phase of the response of a Si tip on a HOPG sample at 60 nm separation are obtained following the procedure in section 3.1. The results are shown in Figure 7. In Figure 7 discontinuities can be observed in the amplitude and phase at specific driving frequencies and finite jumps occur on and off a "saturated" amplitude branch. The cantilever response on this branch is highly nonlinear with higher harmonics of the excitation present in the response as the tip impacts the sample. The jumps J1, J2, J3, and J4 in Figure 7 render hysteretic the response of the cantilever when the driving frequency is swept up and down.

The computed results in AUTO using system parameters from Table 1 are shown in Figure 8. The amplitude and phase (of the first harmonic of motion with respect to base motion) as a function of excitation frequency for the specific value of $\bar{y} = 0.0145$ chosen in the experiment.

The initial softening and subsequent hardening of the forced vibration response then leads to the occurrence of periodic folds or global saddle node (SN) bifurcations [26] at points SN1, SN2, SN3, SN4 in Figure 8. Each bifurcation corresponds to the creation or the destruction of a pair of a stable (indicated by solid lines) periodic orbit and an unstable periodic orbit (indicated by dotted lines). This leads directly to the observed jumps and hysteretic behaviors in Figure 7 because as a frequency sweep is performed in Figure 8, the response follows a stable solution up to a bifurcation point where it jumps to another stable branch which lies in its basin of attraction. This response is typical of the *monostable* region. The physical reasons for this nonlinear response have been discussed in detail in recent work of the authors [27] and are not discussed here. It suffices to note that the softening nonlinear response is due to the attractive van der Waals forces and the hardening part of the response is due to the nanoscale contact mechanics.

The computational results reproduce very closely the experimentally observed

response (Figure 7). As the frequency is increased from below resonance, the computed periodic solution follows the stable branch and jumps into another stable branch at SN1 and SN3 in Figure 8. Likewise during a frequency sweep-up the experimentally measured response in Figure 7 follows the solid dots leading to jumps at J1 and J3. Similarly the computed response during a decrease of excitation frequency from above resonance jumps at SN4 and SN2 (Figure 8) and the experimentally measured response during frequency sweep down (circles in Figure 7) encounters jumps at J4 and J2.

Clearly there is a good agreement between theory and experiment as far as amplitude response and the locations of the jumps is concerned. However, differences in computed and experimental phase response are noticeable and are most likely a reflection of inadequate modeling of dissipation during contact. It may be noted that during tapping mode the response contains higher harmonics also, and the phase is computed with respect to the first harmonic.

4.2 Response in bistable region

Next consider the response in the *bistable* region which is located closer to the surface. Note that the bistable region for the experimental tip was small so that inherent thermal drifts during the experiment caused the tip to stick to the sample before the near resonance response was measured. In this case therefore it is difficult to perform the nonlinear response experiments. Instead the computed response in Figure 9 is presented from 0 to 80 kHz for the specific value of $\bar{y} = 0.175$ at the approach distance $Z = 5$ nm.

The nonlinear amplitude response in Figure 9 is softening only and it destabilizes through period doubling (PD) bifurcations. Also the softening of the response leads to the occurrence of global saddle node (SN) bifurcations at points SN1 and SN2 in Figure 9. Period doubling bifurcations, which are not detected in the *monostable* region for the chosen parameter values, can occur leading to the generation of subharmonics in the response [18,28]. The extremely softening response with period doubling and global saddle node bifurcations in the *bistable* region creates a frequency range between SN1 and PD2 wherein no stable periodic orbits exist about the chosen equilibrium. In this region of instability the tip can escape the local potential well to execute complex cross well dynamics or stick to the sample (i.e. be captured by the other coexisting equilibrium). To demonstrate this effect MATLAB simulations are performed at excitation frequencies 59.212 kHz and at 60.784 kHz in the bistable region with an approach distance of 5 nm (see Figure 9). Specifically initial conditions are taken from the AUTO computed stable periodic solution at 60.784 kHz and from the unstable periodic solution at 59.212 kHz. The corresponding phase portraits of the simulations are shown in Figure 10

(a) and (b). In both phase portraits the initial condition is indicated by a solid dot. In Figure 10 (b) the chosen initial condition leads to a stable periodic solution about the equilibrium located further from the surface. However the initial conditions starting on the unstable periodic solution in Figure 10 (a) eventually escape the potential well and execute a periodic motion about the equilibrium closer to the surface. The amplitude of this resulting periodic motion is exactly that of the base excitation Y. This together with the fact that these equations are written in a co-moving frame imply that the tip simply escapes the local potential well and sticks to the sample.

The response in the *bistable* region therefore is completely different from that in the *monostable* region.

4.3 Bifurcation sets

Thus far the nonlinear response of the microcantilever has been discussed for representative approach distances in the *monostable* and *bistable* regions. Consider now the ensemble of measured and computed nonlinear responses at all intervening approach distances. Figure 11 show the experimental and computed amplitude and phase response for excitation frequency varying across resonance, for different approach distances, while maintaining constant the excitation amplitude Y. Note that the excitation amplitude $\bar{y}$ in equation (6) is nondimensionalized with respect to the equilibrium gap between the tip and the sample. Thus while Y is held constant at different approach distances, $\bar{y}$ proportionally increases as the cantilever is brought closer to the sample.

First when the approach distance Z is large over 100 nm, the response is linear as shown in Figure 11. However as the tip approaches the sample, it starts tapping the sample in the *monostable* region. The saturated amplitude region and the corresponding bifurcations can be clearly seen in Figure 11(c, d), which agrees well with the experimental response in Figure 11(a, b). When the tip is brought closer to the sample, it is in the *bistable* region. The response in this region shows a softening nonlinear response and includes destabilizing period doubling bifurcations as shown in section 4.2.

To describe the different regimes of nonlinear response better in the approach distance Z and the excitation frequency Ω parameter plane, the bifurcation points can be projected onto $Z - \Omega$ parameter space. The loci of the resulting saddle node and period doubling bifurcations projected on $Z - \Omega$ parameter parameter space are the bifurcation sets of the system. Note that the loci of the period doubling bifurcations are expected to appear in the *bistable* region. Figure 12(a) shows the global structure of the bifurcation sets, while Figure 12(b) is a detailed view of the bifurcation sets near resonance in the

$Z-\Omega$ parameter space. Several observations can be made from the bifurcation sets:

(1) All the saddle node bifurcation sets SNS1, SNS2, SNS3, and SNS4 appear near resonance. However, SNS1 and SNS2 corresponding to the softening nonlinear response are created simultaneously below resonance, while SNS3 and SNS4 are created above resonance.
(2) The saddle node bifurcation sets SNS2 and SNS4 merge near zero frequency as Z decreases in the *bistable* region. As Z decreases further from this point, only SNS4 exists in the low frequency range. This indicates that SNS2 is likely "pinched-off" from the main resonant branch onto an isola.
(3) The saddle node bifurcation set SNS3 is suddenly discontinued as Z decreases in the *bistable* region. This also supports the previous suggestion of the existence of an isola of periodic motions which cannot be detected computationally on the primary resonant branch while using the excitation frequency as the lone continuation parameter.
(4) The period doubling bifurcation sets PDS exist only in the *bistable* region for the chosen parameter values. One branch of PDS is located very close to SNS4 and follows SNS4. This suggests that there is a rapid variation of Floquet multipliers near the onset of SN4.

The construction of the bifurcation sets predict clearly the response of the system in the constant excitation frequency, varying approach distance case (DFM). As one approaches the sample while maintaining fixed the excitation frequency and dither amplitude, one is traversing the bifurcation sets in Figure 12(b) along a straight line in the $Z-\Omega$ parameter space corresponding to a fixed excitation frequency.

5 Implications for dynamic force microscopy

The experimental DFM responses (rms amplitude and phase of the first harmonic) are shown in Figure 13. Figure 13 corresponds to DFM responses with fixed excitation frequency below resonance, at resonance, and above resonance, respectively. These results are typical of DFM response near resonance. The experimental results in Figure 13 are performed with the identical tip and sample used in the previous experimental results in Figure 11. However, the excitation amplitude is greater (1.5 times) than that used previously. Nonetheless, the previously computed bifurcation sets clearly explain qualitatively the experimental results observed in DFM (the fixed frequency, varying approach

distance scenario) as follows:

(1) If the excitation frequency is fixed at linear resonance (here at 52.4 kHz) while the tip approaches and retracts from the sample, this corresponds in the $Z-\Omega$ parameter space to the straight line $A-A$ shown in Figure 12(b). Clearly this line does not intersect any bifurcation set in the *monostable* region. Therefore no jumps are to be expected as the tip approaches and retracts from the sample. This result corresponds to the experimental result in Figure 13(b).
(2) If excitation frequency is slightly greater than resonance (for example, 52.6 kHz), we approach the sample along the line $B - B$ shown in Figure 12(b). We encounter first SNS4 during approach in the *monostable* region. During retraction, SNS3 is encountered in the *monostable* region. Thus we can expect two jumps to take place in the *monostable* region as the tip approaches and retracts from the sample.
(3) If the excitation frequency is slightly below resonance (for example, 52.0 kHz) then we approach the sample along the following line $C - C$ shown in Figure 12(b). Clearly we encounter SNS1 first during approach and SNS2 upon retraction. This leads to the hysteretic jumps in *monostable* region as shown in Figure 13(a).

Note that the jumps for the below and above resonance cases, occur at different approach distance from the sample. Also note that in all three cases above, if the tip is brought even closer to sample during the approach in the *bistable* region, we may cross the period doubling bifurcation set. This leads eventually to the tip either sticking to the sample or tapping irregularly the sample. The experiments in Figure 13 indicate that upon reduction of Z into the bistable region, the tip invariably eventually escapes the potential well to stick to the sample.

6 Conclusions

In conclusion, because the shape of tip-sample interaction potential well is fundamentally dependent on Z, the nonlinear response of the tip also depends on Z. Therefore the dynamics in the monostable and bistable regions are very different.

The use of computational continuation techniques with realistic parameter values from experiment and a vdW/DMT contact model - lead to excellent quantitative comparison between theory and experiment for the monostable region as far as the amplitude response is concerned. Differences in phase response indicate the need for better modeling of dissipation during contact.

The nonlinear response at each Z in the monostable region consists of jumps or saddle node bifurcations. The frequency at which these bifurcations occur depends on Z. Bifurcation sets are obtained by plotting the loci of the bifurcation points in the approach distance - excitation frequency parameter space. The nonlinear response in dynamic force microscopy is conveniently predicted through observation of the bifurcation sets intersected during approach and retraction.

Acknowledgements

The corresponding author (AR) acknowledges the support of the National Science Foundation (NSF) under Award No. 0116414-CMS. Dr. Alison Flatau is the program manager. One of the authors (RR) would like to thank Prof. Julio Gómez-Herrero and Prof. Jaime Colchero for their continued help with the NanoTec^{TM} WSxM software.

References

[1] G. Haugstad, R. R. Jones, Ultramicroscopy 76 (1999) 77.

[2] M. Lantz, Y. Z. Liu, X. D. Cui, H. Tokumoto, S. M. Linsay, Surf. Interface Anal. 27 (1999) 354.

[3] P. J. de Pablo, J. Colchero, M. Luna, J. Gómez-Herrero, A. M. Baró, Phys. Rev. B 61 (2000) 14179.

[4] X. Chen, M. C. Davies, C. J. Roberts, S. J. B. Tendler, P. M. Williams, N. A. Burnham, Surf. Sci. 460 (2000) 292.

[5] A. San Paulo, R. García, Biophys. J. 78 (2000) 1599.

[6] R. García, A. San Paulo, Phys. Rev. B 61 (2000) R13381.

[7] R. García, A. San Paulo, Ultramicroscopy 82 (2000) 79.

[8] B. Anczykowski, D. Krüger, K. L. Babcock, H. Fuchs, Ultramicroscopy 66 (1996) 251.

[9] L. Nony, R. Boisgard, J.-P. Aimé, Eur. Phys. J. B 24 (2001) 221.

[10] P. Gleyzes, P. K. Kuo, A. C. Boccara, Appl. Phys. Lett. 58 (1991) 2989.

[11] A. Kühle, A. H. Sørensen, J. Bohr, J. Appl. Phys. 81 (1997) 6562.

[12] R. García, A. San Paulo, Phys. Rev. B 60 (1999) 4961.

[13] M. Marth, D. Maier, J. Honerkamp, R. Brandsch, G. Bar, J. Appl. Phys. 85 (1999) 7030.

[14] B. V. Derjaguin, V. M. Muller, Y. P. Toporov, J. Colloid Interface Sci. 53 (1975) 314.

[15] U. Rabe, K. Janser, W. Arnold, Rev. Sci. Inst. 67 (1996) 3201.

[16] L. Meirovitch, Principles and Techniques of Vibrations, Prentice Hall, 1997.

[17] A. Ulcinas, V. Snitka, Ultramicroscopy 86 (2001) 217.

[18] W. van de Water, J. Molenaar, Nanotechnology 11 (2000) 592.

[19] M. V. Salapaka, D. J. Chen, J. P. Cleveland, Phys. Rev. B 61 (2000) 1106.

[20] A. Kühle, A. H. Sørensen, J. B. Zandbergen, J. Bohr, Appl. Phys. A 66 (1998) S329.

[21] A. San Paulo, R. García, Phys. Rev. B 64 (2001) 193411.

[22] M. Gauthier, N. Sasaki, M. Tsukada, Phys. Rev. B 64 (2001) 085409.

[23] B. Gotsmann, H. Fuchs, Phys. Rev. Lett. 86 (2001) 2597.

[24] D. Sarid, Scanning Force Microscopy: with applications to electric, magnetic and atomic forces, Oxford University Press, 1991.

[25] J. Israelachvili, Intermolecular and surface forces, Academic Press, 1992.

[26] J. Guckenheimer, P. Holmes, Nonlinear oscillations, dynamical systems and bifurcations of vector fields, Springer Verlag, 1991.

[27] S. I. Lee, S. W. Howell, A. Raman, R. Reifenberger, submitted .

[28] N. A. Burnham, A. J. Kulik, G. Gremaud, G. A. D. Briggs, Phys. Rev. Lett. 74 (1995) 5092.

Table 1
Constants and properties of the Si microcantilever and HOPG sample used in numerical computation.

Description	Value
Tip radius	$R = 20$ nm
Cantilever length	$L = 240$ μm
Cantilever width	$b = 64$ μm
Cantilever thickness	$h = 2.1$ μm
Cantilever material density	$\rho_c = 2300$ kg/m^3
Cantilever Young's modulus	$E_c = 176$ GPa
Effective elastic modulus	$E^* = 10.4$ GPa
Static bending stiffness	$k = 2.0$ N/m
1st natural frequency	$f_1 = 52.4$ kHz
Q factor (in air)	$Q = 66.7$
Hamaker constant (Si-HOPG)	$A = 2.96 \times 10^{-19}$ J
Intermolecular distance	$a_0 = 2.0$ Å

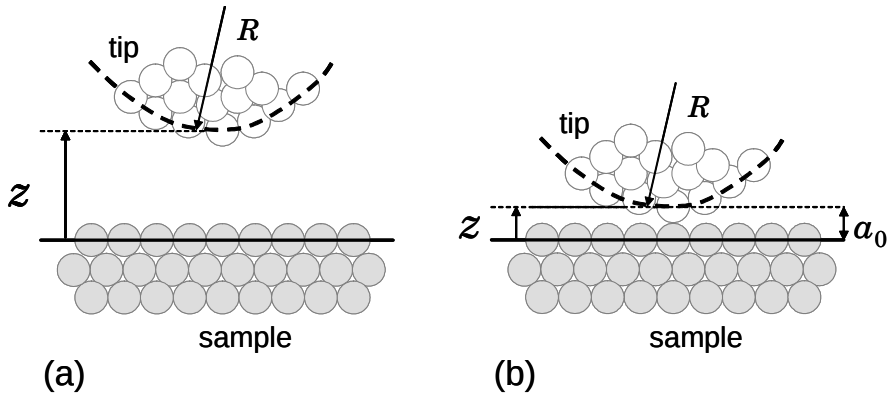

Fig. 1. Two different tip-sample interaction regimes: (a) when the tip is located far from the sample; and (b) when the tip-sample contact is initiated.

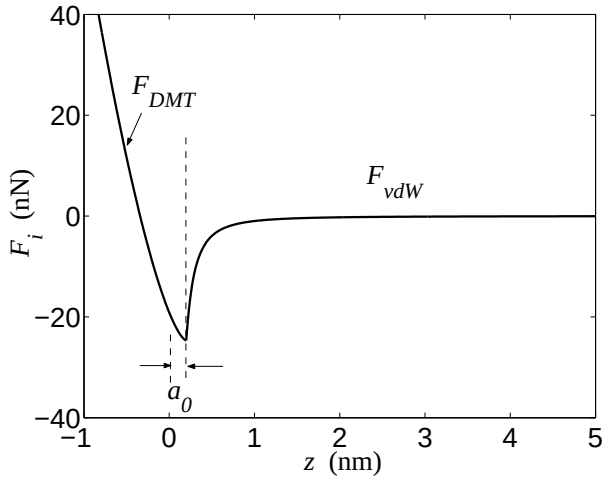

Fig. 2. Interaction model described by van der Waals and DMT contact forces. The interaction can be divided into two regimes: van der Waals force regime (Equation (1)) and DMT contact regime (Equation (2)). Negative interaction implies attractive force, whereas positive interaction in contact regime represents repulsive or elastic restoring force.

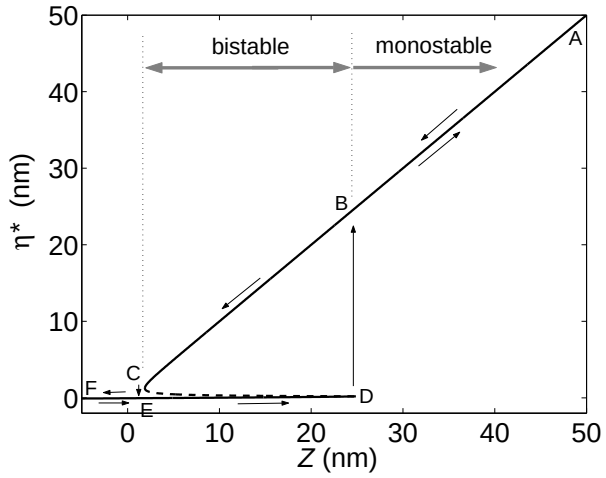

Fig. 3. Equilibrium solutions of the nonlinear equilibrium and their stability. The solid lines represent Liapunov stable solutions while the dashed line indicates an unstable equilibrium. Tip-sample approach: $A \rightarrow B \rightarrow \mathrm{C} \rightarrow E \rightarrow F$. Tip-sample retraction: $F \rightarrow E \rightarrow D \rightarrow B \rightarrow A$.

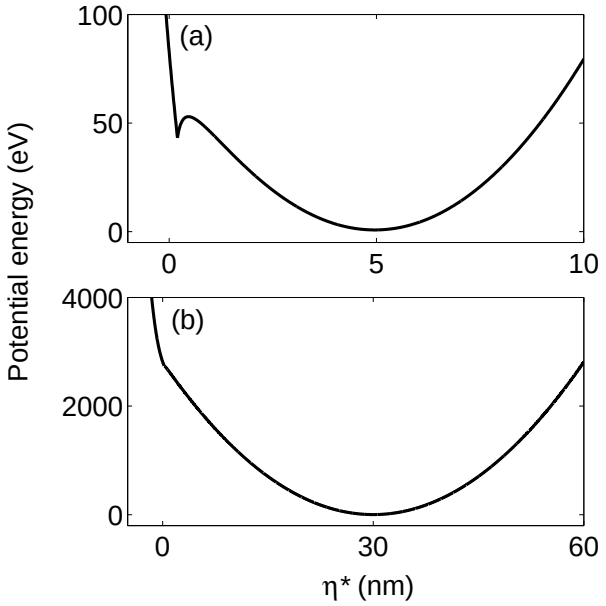

Fig. 4. Total potential energy wells: (a) asymmetric two-well potential in *bistable* region (at $Z = 5$ nm); (b) single well potential with contact in *monostable* region (at $Z = 30$ nm).

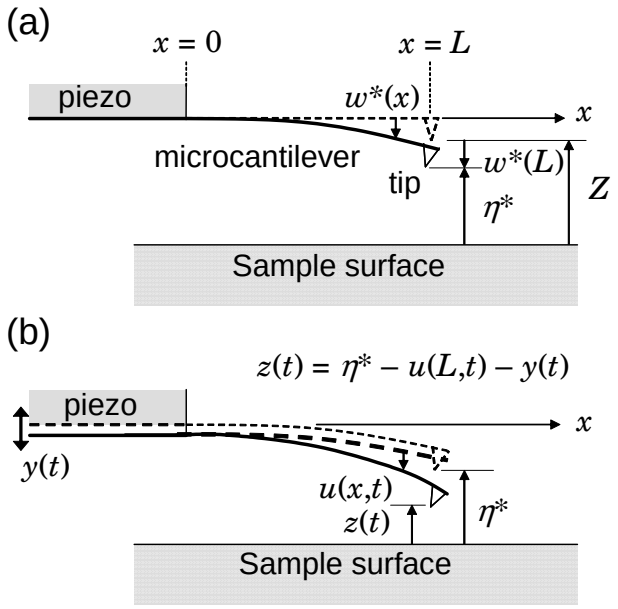

Fig. 5. Schematic diagram of the cantilever configurations. (a) Initial statically deflected configuration under van der Waals tip forces. Z is the approach distance in the absence of van der Waals forces. (b) Dynamic (current) configuration as cantilever vibrates about its elastostatic equilibrium.

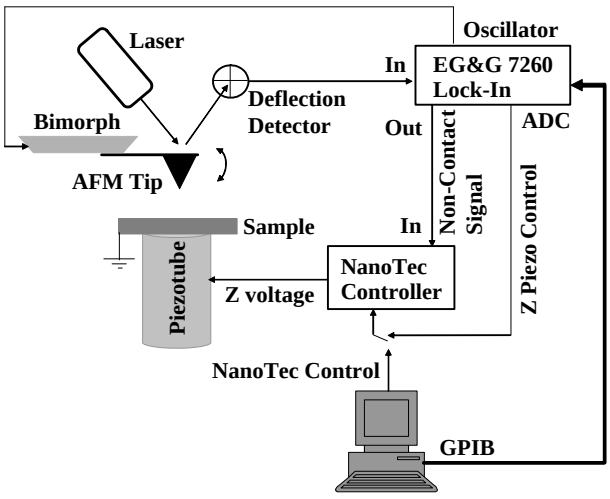

Fig. 6. A schematic diagram of the experimental setup for measuring the nonlinear behavior near resonance of microcantilevers interacting with samples.

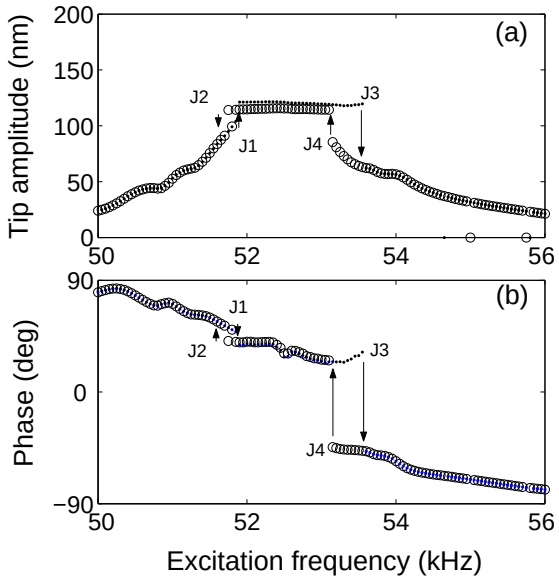

Fig. 7. Experimental amplitude and phase (w.r.t. driving frequency) response of the silicon tip on HOPG sample. Nonlinear tip amplitude (a) and phase (b) response with 60 nm tip-sample approach distance (in *monostable* region). Dots: response during frequency sweep up; Circles: response during frequency sweep down. The arrows indicate the abrupt discontinuities in amplitude and phase that are important signatures of the nonlinear interaction potential. Tip amplitude indicates the peak-to-peak tip oscillation amplitude of the microcantilever.

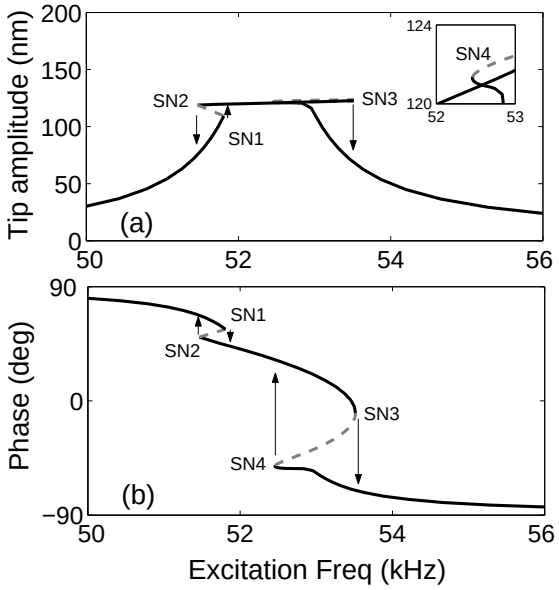

Fig. 8. The response prediction in *monostable* region using periodic solution continuation and stability routines in AUTO. Solid/dotted lines indicate stable/unstable solutions, respectively. In (a), tip amplitude indicates the peak-to-peak tip oscillation amplitude of the microcantilever. In (b), phase between the first harmonic of response and the base excitation is computed in AUTO.

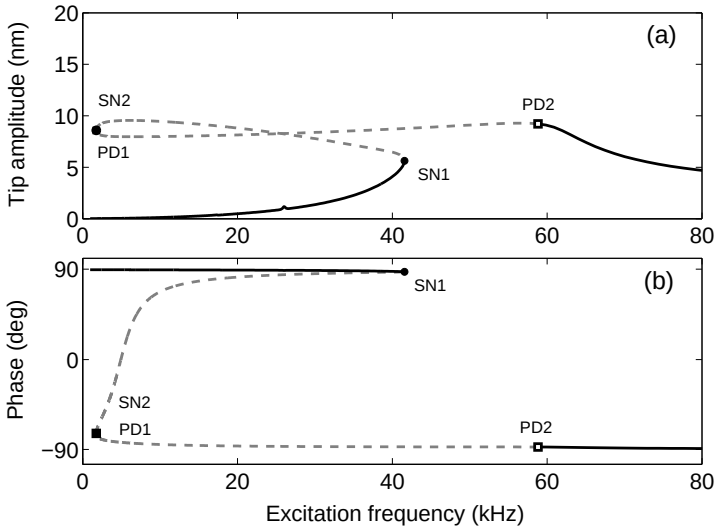

Fig. 9. The predicted response in *bistable* region ($Z = 5$ nm) using periodic solution continuation and stability routines in AUTO. Solid/dotted lines indicate stable/unstable solutions, respectively. In (a), tip amplitude indicates the peak-to-peak tip oscillation amplitude of the microcantilever. In (b), phase between the first harmonic of response and the base excitation is computed in AUTO.

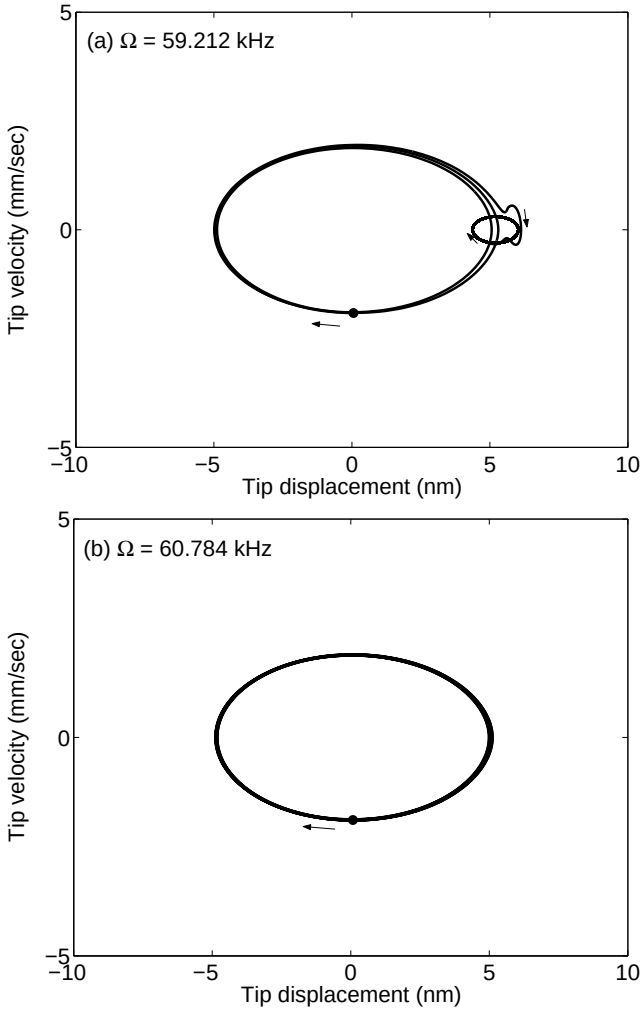

Fig. 10. Computed phase portraits of tip response in the *bistable* region ($Z = 5$ nm). (a) Evolution of initial conditions located on the unstable periodic solution at 59.212 kHz excitation frequency. (b) Evolution of initial conditions located on the stable periodic solution at 60.784 kHz excitation frequency. In (a), the tip escapes from the local potential well to stick to the sample.

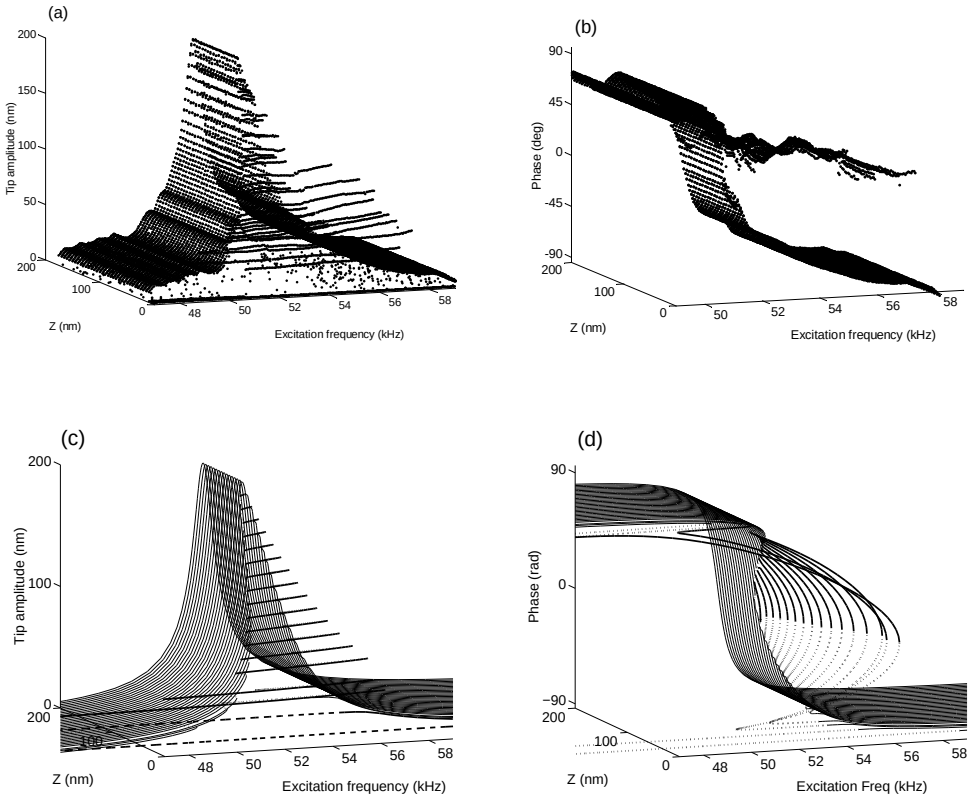

Fig. 11. Experimental peak-to-peak amplitude (a) and phase (b) response for various approach distances of the Si cantilever - HOPG sample system. In (a, b), responses during frequency sweep up and down are indicated by the same symbol (dot). Computational peak-to-peak amplitude (c) and phase (d) response using AUTO for various approach distances of the Si-HOPG system. In (c, d), solid/dotted lines indicate stable/unstable solutions, respectively. Phase in (d) is computed between the first harmonic of response and the base excitation.

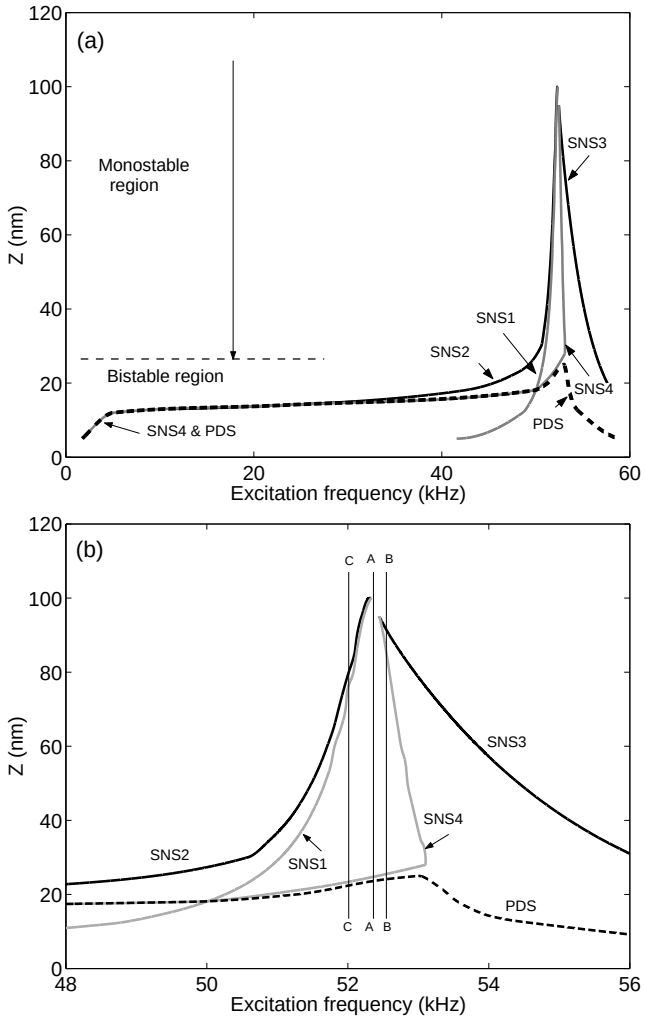

Fig. 12. (a) Bifurcation sets projected on the approach distance-excitation frequency ($Z - \Omega$) parameter space. Solid lines indicate the global saddle node bifurcation (or period folds) sets (SNS), and dotted lines indicate period doubling bifurcation sets (PDS). (b) Detailed view near resonance. In (b), the vertical lines A-A, B-B, and C-C indicate the fixed frequency, varying approach distance scenarios at resonance, above resonance, and below resonance, respectively.

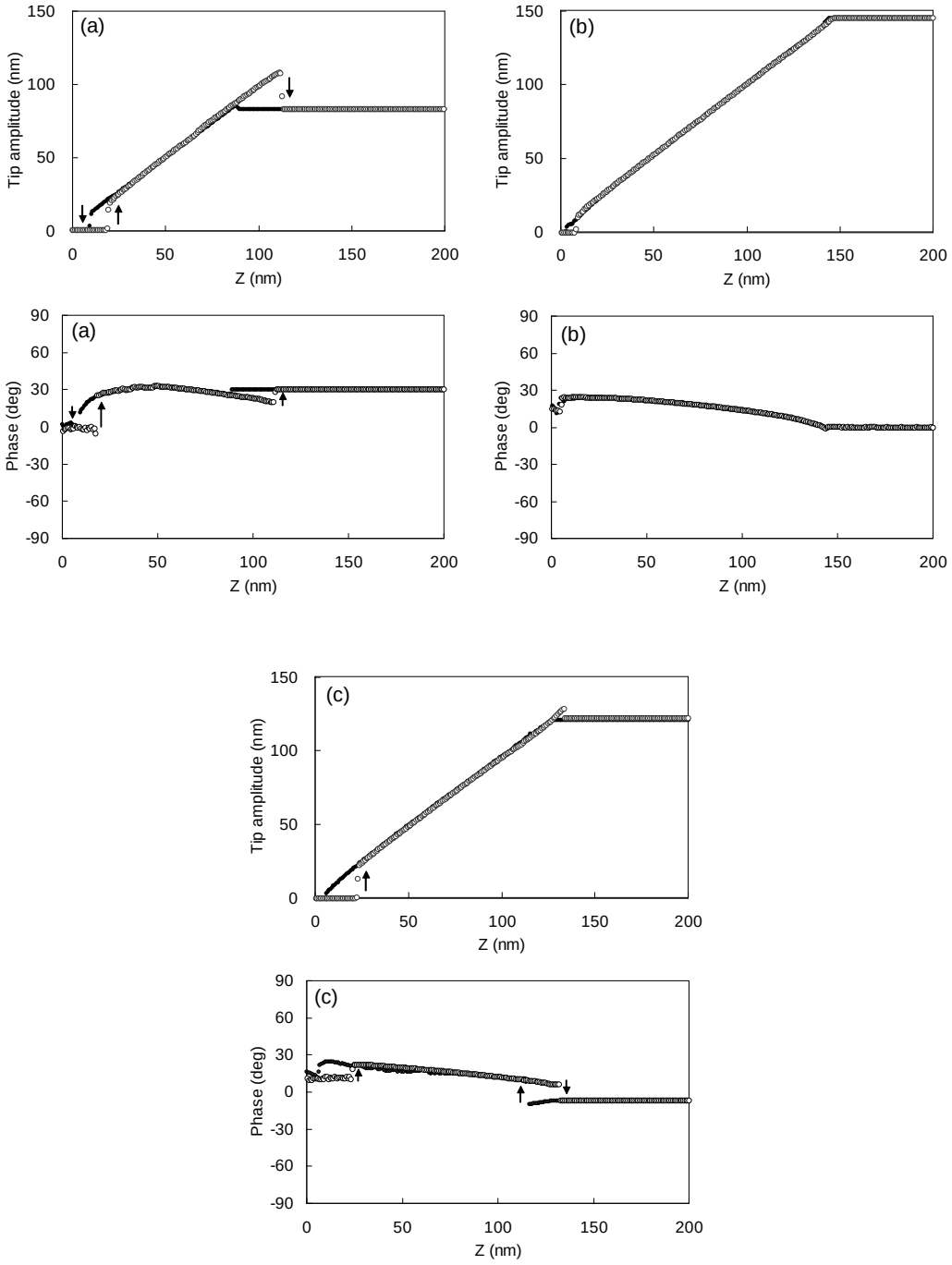

Fig. 13. Experimental DFM response (rms amplitude and phase) for the fixed frequency, varying approach distance scenario: (a) below resonance (52.0 kHz), (b) at resonance (52.4 kHz), (c) above resonance (52.6 kHz). Dots: response during tip approach; Circles: response during tip retraction.